Applied Catalysis B: Environmental 127 (2012) 59–67

Contents lists available at SciVerse ScienceDirect

Applied Catalysis B: Environmental

journal homepage: www.elsevier.com/locate/apcatb

Cobalt hydrotalcites as catalysts for bioethanol steam reforming. The promoting effect of potassium on catalyst activity and long-term stability

Raúl Espinal[a], Elena Taboada[a], Elies Molins[b], Ricardo J. Chimentao[c], Francesc Medina[c], Jordi Llorca[a,*]

[a] Institut de Tècniques Energètiques and Centre de Recerca en Nanoenginyeria, Universitat Politècnica de Catalunya (UPC), Av. Diagonal, 647, 08028 Barcelona, Spain
[b] Institut de Ciència de Materials de Barcelona (ICMAB-CSIC), Campus UAB, 08193, Bellaterra, Spain
[c] Escola Tècnica Superior d'Enginyeria Química, Universitat Rovira i Virgili (URV), Av. Països Catalans, 26, 43007 Tarragona, Spain

ARTICLE INFO

Article history:
Received 15 June 2012
Received in revised form 25 July 2012
Accepted 9 August 2012
Available online 16 August 2012

Keywords:
Hydrogen
Ethanol reforming
Bioethanol
Cobalt catalyst
Hydrotalcite-derived catalyst
Honeycomb

ABSTRACT

Cobalt hydrotalcite-derived catalysts, doped with potassium, are active materials for the ethanol steam reforming reaction. Potassium addition reduces the acid sites number and strength. It acts as a promoter of the ethanol steam reforming (ESR); ethanol conversion is higher at lower temperature, as the amount of potassium at the surface of the catalyst increases. The catalysts are stable for long-term experiments (300 h) under high loads of ethanol and bioethanol (0.036 g_{EtOH} min^{-1}, H_2O:CH_3CH_2OH = 4:1 molar). Moreover, they generate a low amount of carbon (0.0067 g_C $g_{catalyst}^{-1}$ h^{-1}). The catalysts after reaction contain almost exclusively high spin Co^{2+} in cobalt oxide (or in (Co,Mg)O); only traces of metallic cobalt are identified by magnetometry, <0.1 wt.% Co^0, suggesting that oxidized cobalt is an active species in ESR.

1. Introduction

Hydrogen production from ethanol steam reforming (ESR) reaction has great interest because it allows obtaining six molecules of hydrogen from one molecule of ethanol and three molecules of water:

$$C_2H_5OH + 3H_2O \rightarrow 6H_2 + 2CO_2 \quad (1)$$

Bioethanol is produced from biomass fermentation, for what it is a renewable energy source. Bioethanol is then CO_2 neutral within the reforming reaction, because the carbon dioxide produced in this reaction comes from the carbon dioxide absorbed from the biomass during its growth.

For ESR, the use of suitable catalysts allows total conversion of ethanol at lower temperatures and better selectivity towards hydrogen, with reduced production of undesirable side-products. Catalysts based on noble metals are optimal to avoid coke formation [1]. However, they are very expensive and need high temperatures to be active (923–1023 K). On the other hand, cobalt-based catalysts are cheap and active at low temperatures (523–823 K), but they deactivate quickly due to coke generation. Coke formation is associated with metallic nanoparticles, which nucleate the growth of carbon nanotubes [2]. It is generally accepted that metallic cobalt is the active species for the ESR, being essential for the reaction, but also that the redox pair $Co^0 \rightleftarrows Co^{2+}$ is responsible for the activity of cobalt in ESR [3–6]. Casanovas et al. pointed out that the easy exchange between oxidized and reduced cobalt centres may promote catalytic activity of Co-ZnO not only in ESR but also in WGS, where water behaves both as a reactant and as an oxidant [7]. Busca et al. also found that the presence of oxidized cobalt increased the selectivity towards H_2 and CO_2 over Ni-Co-Zn-Al catalysts. Their data suggested that the less reduced the surface, the more favoured is the conversion of ethanol into acetic acid, likely through ethoxy groups and acetaldehyde. Acetic acid and its adsorbed forms as acetate species may be converted to CO_2 on a less reduced surface, while they mostly decompose to methane and CO_x on a highly reduced catalyst [8]. An important advantage of carrying out the ESR at moderate temperature is that WGS occurs simultaneously with steam reforming and consequently CO concentration is kept low. In addition, methane is not an intermediate of the reforming process over Co-based catalysts and, consequently, high hydrogen yields are easy to achieve [7]. CH_4 is a secondary product formed through the methanation reaction [9].

Within this context, the search for cobalt-based catalysts for ESR that do not generate coke and therefore, do not deactivate, is an open issue. Essential for this matter is the understanding of the role of cobalt oxidation state. In one of our previous works, we studied cobalt hydrotalcites as precursors for ESR catalysts [10]. After

* Corresponding author. Tel.: +34 93 4011708; fax: +34 93 4017149.
E-mail address: jordi.llorca@upc.edu (J. Llorca).

0926-3373/$ – see front matter © 2012 Elsevier B.V. All rights reserved.
http://dx.doi.org/10.1016/j.apcatb.2012.08.006

calcination at 823 K, they are converted to cobalt spinels, which are very active. Ethanol conversion was total at 823 K, reaching 70% of hydrogen selectivity (S/C = 2, W/F = 390 to 10^4 g min mol_{EtOH}^{-1}) and, more interestingly, coke formation was minor. We analysed the samples after reaction by several techniques (magnetometry, XRD, X-ray photoelectron spectroscopy (XPS), HRTEM, etc.) and we observed traces of metallic cobalt only by magnetometry (between 5.9 and 0.1 wt.% Co^0, depending on the metallic molar fraction of the hydrotalcite); no metallic cobalt was detected by X-ray diffraction, neither by in situ XPS and HRTEM. Therefore, we concluded that the main active species in ESR was oxidized cobalt. This interesting result allows designing catalysts containing cobalt for ESR without coke deposition (no metallic cobalt) by placing in appropriate environments Co^{2+} active species. A similar conclusion has been reached by da Costa-Serra and Chica [11] using delaminated zeolite as Co support.

Here, we present a further study of cobalt hydrotalcites which were doped with potassium at several weight percentages. The hydrotalcite with molar composition Co:Mg:Al = 1:2:1 was chosen to be doped with potassium because it showed the better catalytic activity in the former study [10]. The aim of the potassium doping was to reduce even more the coke formation, by neutralizing the acid sites of the hydrotalcites, which are likely the responsible for ethanol dehydration into ethylene and other coke precursors. The catalysts are active for ESR, with high stability in time and little coke formation. Potassium acts as a promoter of the reaction, favouring the ethanol conversion at lower temperature. No metallic cobalt was observed by XPS after reaction and less than 0.1 wt.% by magnetometry. Then, oxidized cobalt appears once more as an active species for ethanol reforming. The catalytic tests were directly carried out over monoliths washcoated with the catalysts to simulate practical application. For the same reason, the performance of the catalytic monoliths was also tested with commercial bioethanol.

2. Experimental

2.1. Catalyst preparation

The Co/Mg/Al hydrotalcite with formula $[Co_2Mg_4Al_2(OH)_{16}]CO_3{\cdot}4H_2O$ (Co:Mg:Al molar ratio = 1:2:1) was prepared by the co-precipitation method. Briefly, aqueous solutions of an appropriate amount of $Co(NO_3)_2{\cdot}6H_2O$, $Mg(NO_3)_2{\cdot}6H_2O$ and $Al(NO_3)_3{\cdot}9H_2O$ precursors and 2 M NaOH alkaline solution were separately prepared. These solutions were then simultaneously added drop-wise into 100 ml of deionized water maintaining a constant pH (10 ± 0.5) under vigorous mechanical stirring. After the co-precipitation, the suspension was aged overnight under stirring at room temperature, filtered, and thoroughly washed with deionized water. The resulting solid was then dried overnight at 373 K and calcined at 723 K for 12 h to obtain the hydrotalcite-derived mixed oxides.

Potassium addition to the calcined hydrotalcite (over the same batch) was accomplished by impregnation with a 0.032 M KOH aqueous solution. Three samples with different amount of potassium were prepared: 0.5, 1.0 and 2.0 wt.%, referred to the nominal cobalt content. The resulting materials were dried at 373 K and calcined at 723 K for 4 h. The potassium was introduced after the formation and calcination of the hydrotalcite, instead of co-precipitating the potassium salt together with the other metal salts or instead of impregnating the hydrotalcite previous to calcination, to favour its deposition at the surface of the mixed oxides. The samples will be referred from now on as 0K_calc (reference sample with no potassium), 0.5K_calc, 1K_calc and 2K_calc, respectively.

The calcined hydrotalcites were deposited onto cordierite supports (400 cells per square in.) by the washcoating method. Honeycombs were from Rauschert Company, with a nominal chemical composition of $Al_3Mg_2AlSi_5O_{18}$. They were cut into cylindrical pieces of 1.8 cm in diameter and 2 cm long. A 5:1 molar mixture of polyvinyl alcohol (PVA) and acetic acid was used as binding agent. The resulting catalytic honeycombs were dried at 363 K for 2 h and calcined at 823 K for 3 h. The washcoating procedure was repeated several times until the catalyst loading was ca. 5% with respect to the cordierite support.

2.2. Catalytic tests

ESR was carried out in the temperature range 523–823 K (every 50 K) at atmospheric pressure in a tubular stainless-steel reactor over the catalytic honeycombs without any pre-treatment. The reaction was first tested with a gaseous H_2O:CH_3CH_2OH = 4:1 molar mixture (steam to carbon, S/C = 2) by using a nitrogen stream saturated with the reactants (8.0×10^{-5} g_{EtOH} min^{-1}, W/F = 13.4×10^3 g min mol_{EtOH}^{-1}). Stability tests were then conducted at 823 K with pure liquid mixtures of absolute ethanol (Sigma–Aldrich) and commercial bioethanol (Deulep, 1 ppm sulphur, 300 ppm 4-methylpentane-2-ol, 100 ppm methanol, 30 ppm acetic acid, 20 ppm ethyl acetate, 10 ppm acetaldehyde, 2 ppm benzene, 25 ppm non-volatile residue), provided directly with a Knauer Smartline HPLC pump (the liquid mixture was vaporized at 450 K before entering the reactor; S/C = 2, 0.018 g_{EtOH} min^{-1} for 7 h long stability tests and 0.036 g_{EtOH} min^{-1} for 300 h long stability tests). VHSV values ranged from 325 to 625 h^{-1} and W/F values ranged from 475 to 115 g min mol_{EtOH}^{-1}, for 7 and 300 h, respectively. The reactor effluent was monitored on-line every 5 min by gas chromatography (Agilent 3000 A) using MS 5 Å, Plot U and Stabilwax columns. On the other hand, 0K_calc, 0.5K_calc, 1K_calc and 2K_calc powder samples were subjected to ESR at 823 K for 8 h with pure liquid mixture in a similar manner than monoliths, to enable extra *ex situ* characterization. The resulting samples, both monoliths and powder, were labelled as 0K_reac, 0.5K_reac, 1K_reac and 2K_reac.

2.3. Characterization techniques

Both catalytic monoliths and powder catalysts were characterized with the same techniques and identical results were obtained in all cases. X-ray diffraction (XRD) patterns were collected between 10° and 90° of 2θ using a Bruker D8 instrument equipped with Cu Kα incident radiation (λ = 1.5404 Å) and a graphite monochromator. The reacted samples were analysed between 5° and 60° of 2θ, using a Rigaku Rotaflex RU-200 B, also equipped with a Cu target. All the diffractograms were recorded with a step width of 0.02° and a step time of 1 s.

XPS was performed with a SPECS system equipped with an Al anode XR50 source operating at 150 W and a Phoibos 150 MCD-9 detector. Sample powders were pressed to pellets and then fixed into a special sample holder (no glue was used). Spectra were recorded with pass energy of 25 eV at 0.1 eV steps at a pressure below 6×10^{-12} bar; binding energies were referred to the C 1s signal.

Temperature programmed desorption of ammonia (TPD-NH_3) was performed in a Catalyst Analyzer BELCAT-M (BEL Japan, Inc.), equipped with a thermal conductivity detector (TCD). The samples were pre-treated under argon, heated up to 723 K (10 K min^{-1}) maintained at 723 K for 1 h and cooled down to 373 K. Then, the sample was saturated with pure NH_3 for 10 min (30 ml min^{-1}). After this step, in order to drag out the excess of ammonia (the non-interacting with the catalyst) the sample was flushed with argon at 373 K, until the TCD signal was stabilized. Analysis was then performed by heating up to 1173 K (10 K min^{-1}) under argon. The evolution of gases was also monitored by mass spectrometry,

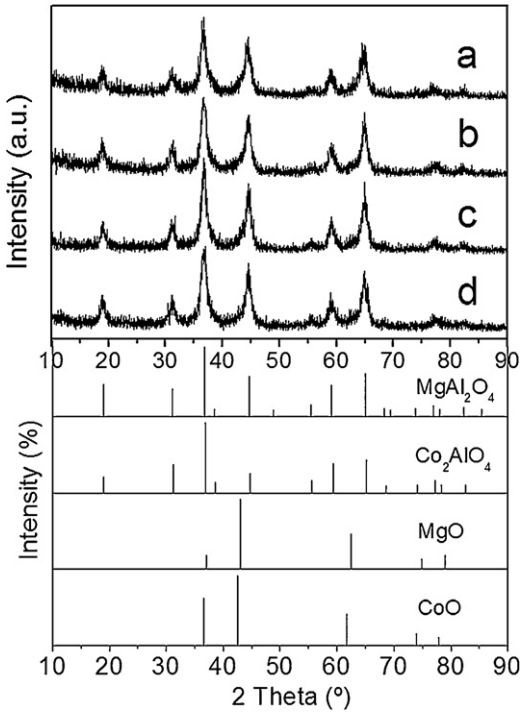

Fig. 1. X-ray diffractograms of samples (a) 0K_calc, (b) 0.5K_calc, (c) 1K_calc and (d) 2K_calc. XRD patterns of several spinel and oxide phases are included for comparison.

with a Cirrus spectrometer from MKS spectra products, equipped with a multiplier detector.

Temperature programmed reduction (TPR) was performed also in a Catalyst Analyzer BELCAT–M (BEL Japan, Inc.). Prior to each TPR run, samples were heated up to 823 K (10 K min^{-1}) and cooled down to room temperature under argon. Then, they were analysed by heating up to 1173 K (10 K min^{-1}) using hydrogen (10 vol% in argon) under a flow rate of 30 ml min^{-1}.

Magnetization (M) vs. applied magnetic field (H) (at 5 and 298 K) and ZFC-FC curves (at 50 Oe) were measured with a superconducting quantum interference device (SQUID) magnetometer (Quantum Design MPMS5XL, USA). A given amount of powder was confined in a gelatin capsule (of known mass) and pressed with a given amount of cotton to avoid the powder from moving during the measurement. The diamagnetic contributions of the capsule and the cotton were subtracted from the total magnetization (m_{total}) as follows:

$$M_{powder}\left(\frac{emu}{g}\right) = \frac{m_{total}(emu) - (\chi_{capsule} mass_{capsule} + \chi_{cotton} mass_{cotton})}{mass_{powder}(g)}$$

where χ is the magnetic susceptibility in cgs units: χ(capsule) = -3.39×10^{-7} emu g^{-1} Oe^{-1} and χ(cotton) = -7.79×10^{-7} emu g^{-1} Oe^{-1}.

3. Results and discussion

3.1. Calcined hydrotalcites

The calcined samples were analysed by X-ray diffraction (see Fig. 1). The XRD profiles of the four samples are identical, indicating that the addition of potassium in the studied range does not affect the crystalline phases of the calcined hydrotalcites (compare the XRD profile of the sample 0K_calc with those of the samples with potassium). Taking into account the stoichiometry of the parent hydrotalcite structure, these compounds are formed by a A(II)B(III)$_2$O$_4$ spinel and A(II)O oxide, where A = Mg^{2+}/Co^{2+} and B = Co^{3+}/Al^{3+} [12]. From the information compiled in Fig. 1 it is deduced that the main peaks of the diffractograms can be indexed to $MgAl_2O_4$ and/or Co_2AlO_4 spinels [13,14] (XRD patterns JCPDS 01-075-1798 and JCPDS 00-038-0814, respectively). In addition, the two shoulders at 43° and 63° of 2θ match the main peaks of the rock salt type phase common to MgO and CoO [15,16] (XRD patterns JCPDS 01-07-1525 and JCPDS 01-075-0533, respectively), suggesting the incipient formation of the simple oxides or the double oxide.

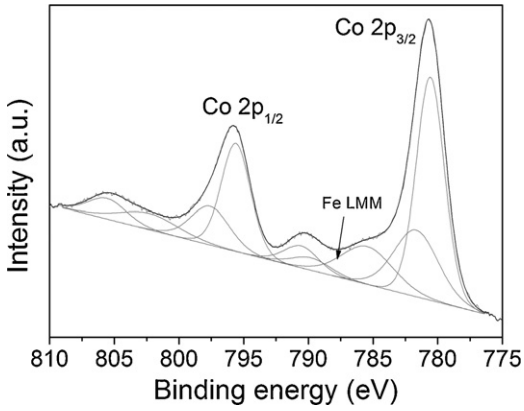

Fig. 2. XP spectrum of sample 1K_calc, representative of the four samples. Residual STD = 1.03.

XP spectra of the calcined samples were analysed in order to determine the oxidation state of the cobalt atoms and to determine the atomic ratio between cobalt and potassium. According to the literature, the Co 2p core-level is composed of two components, Co 2p$_{3/2}$ and Co 2p$_{1/2}$ (which result from the spin orbital splitting) and shake up satellites. XP spectra of the four calcined samples have the same structure at the same energy range: there are two main peaks, the Co 2p$_{3/2}$ and Co 2p$_{1/2}$ photolines, and two weak satellites. The main peaks can be fitted to two components, and the satellites as well (see Fig. 2). A Fe LMM line due to the sample holder is also detected. The first Co 2p$_{3/2}$ component appears at 780.5 eV and can be assigned to an oxidized cobalt species, Co^{n+}. The second component appears at 782.2 eV and might correspond to another cobalt cation in a higher oxidization state than the previous one, or in another atomic environment. This is compatible with the existence of directly Co_2AlO_4 spinel or with other cobalt spinels and CoO or (Mg,Co)O, according to the XRD results discussed above. As expected, there are no peaks assigned to metallic cobalt, around 777–778 eV.

XPS analysis of the surface revealed that the K/Co atomic ratio did not follow the nominal tendency (see Table 1). On the contrary, the amount of potassium at the surface followed the series: 0 < 0.5 < 2 < 1, being the experimental atomic percentage of K/Co at the surface: 0, 0.31, 0.41 and 0.72 at%, respectively. Also, the surface Co:Mg:Al ratio does not match the molar nominal ratio 1:2:1. Sample 0K_calc has the surface metal ratio closest to the

Table 1
Elemental atomic composition of the surface of the catalysts determined by XPS.

Sample	Co:Mg:Al atomic ratio			K/Co atomic ratio
	Co	Mg	Al	
0K_calc	1	2.8	1.5	0
0.5K_calc	1	3.8	1.9	0.31
1K_calc	1	4.1	2.0	0.72
2K_calc	1	4.2	2.4	0.41

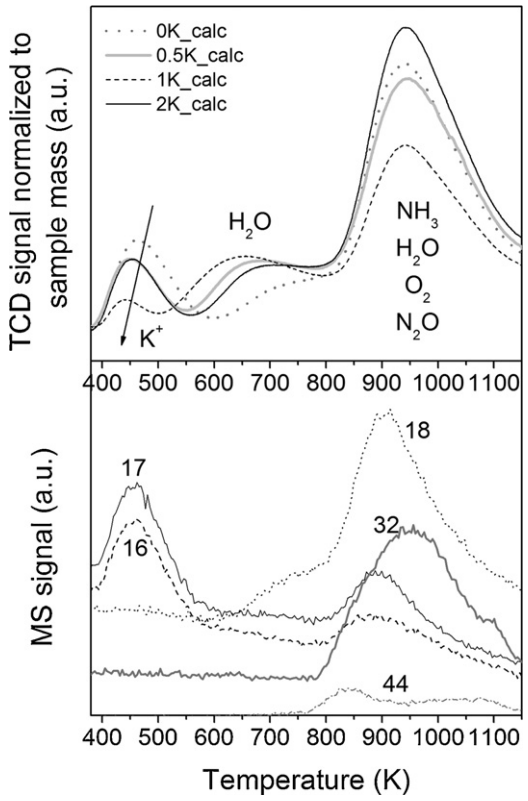

Fig. 3. (Above) TPD-NH_3 profiles of calcined samples with annotation of the evolved gases. (Below) Mass spectrum of sample 0K_calc, coupled to the TPD-NH_3 experiment. Only masses with significant amount are shown.

nominal one: 1:2.8:1.5. Interestingly, as the amount of nominal potassium increases, so does the amount of magnesium and aluminium at the surface, with the corresponding decrease of cobalt (Table 1). These data indicate that the calcination treatment after potassium impregnation (4 h at 723 K) favours the segregation of magnesium and aluminium atoms towards the surface of the calcined hydrotalcite. This has been reported in the literature for K-promoted Co-Cu-Zn-Al catalysts for higher alcohol synthesis [17] and could explain why the K/Co ratio at the surface exhibits a volcano shape with a maximum centred on the 1K_calc catalyst.

Thermal programmed desorption of ammonia (TPD-NH_3) was monitored with mass spectrometry (MS) to calculate the concentration of acid sites at the surface of the material. The TPD profiles present three peaks (Fig. 3). The peak at the lowest temperature, between 433 K and 463 K, corresponds to desorption of ammonia, as evidenced by MS. The second peak is the less intense, between 600 and 700 K, and is related with water evolution. The third peak, which has the largest area, corresponds to several processes: desorption of ammonia ($M = 15^+$ in the mass spectrum), thermal reduction of cobalt with evolution of oxygen ($M = 32^+$), evolution of water ($M = 18^+$, 17^+) and carbon dioxide ($M = 44^+$). This third peak occurred between 939 K and 946 K. No hydrogen and nitrogen evolution was detected at any time, suggesting that there is no decomposition of NH_3 into N_2 and H_2. This has been reported to occur in some ruthenium metal centres [18]. Shen et al. studied the surface acid/base properties of hydrotalcite derived MgAlO oxides by infrared spectroscopy and identified the presence of Brønsted acid sites (H^+) and Lewis acid sites (Al^{3+}) [19]. Considering this information, the peak at the lowest temperature is assigned to NH_4^+ species formed between NH_3 and surface protons. The ammonia evolved at high temperature corresponds to the one anchored at the Al^{3+} ions within the Mg–O–Al species [20]. Interestingly, the area of the first peak decreases as the amount of potassium at the surface (the one determined by XPS) increases. In fact, it follows a linear relationship (see Fig. 4). The amount of acid sites ranges from 0.34 to 0.07 $mmol_{NH_3}\ g_{sample}^{-1}$. Moreover, the temperature of the most intense peak linearly decreases as the amount of potassium at the surface increases, indicating that not only the number of acid sites decreases, but also their strength (see Fig. 3). The intensity of the third peak cannot be directly related to the number of Lewis acid sites, since reduction of cobalt and evolution of CO_2 also takes place. But, taking into account the first peak, our aim of reducing the acid strength of the hydrotalcites by doping with potassium was achieved.

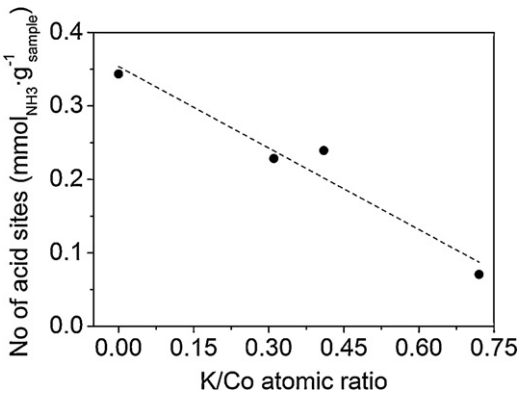

Fig. 4. Amount of acid sites corresponding to the peak centred at 450 K in the TPD-NH_3 profiles vs. K/Co atomic ratio, determined by XPS.

TPR profiles are similar for the four samples (see Fig. 5). Each profile shows two peaks. The first one, which corresponds to the reduction of Co^{3+} to Co^{2+} [10], is centred around 710 K. The second peak appears between 1058 K and 1137 K and corresponds to the total reduction of Co^{2+} to Co^0 [10]. The temperature of the maximum of the second peak decreases as the nominal amount of potassium increases, indicating that potassium doping favours the reduction of the cobalt(II) ions to metallic cobalt. The consumption of hydrogen corresponding to the second peak is ca. four times higher than that associated with the first peak, as expected from the stoichiometry of cobalt spinel (Co_2AlO_4) and/or a mixture of cobalt in other spinels and CoO.

Further characterization by magnetometry was performed on samples 0K_calc and 1K_calc, since they bear the lowest and highest amount of potassium at the surface, as determined by XPS. The magnetic behaviour is the one expected for an antiferromagnetic spinel, as it has been previously observed [21] and in accordance to XRD results. The magnetization at room temperature linearly increased with the magnetic field, as it is expected for a paramagnet (see Fig. 6). At 5 K, the calcined samples behaved slightly

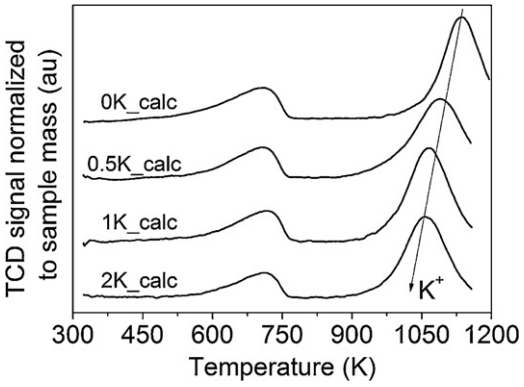

Fig. 5. TPR profiles of calcined samples.

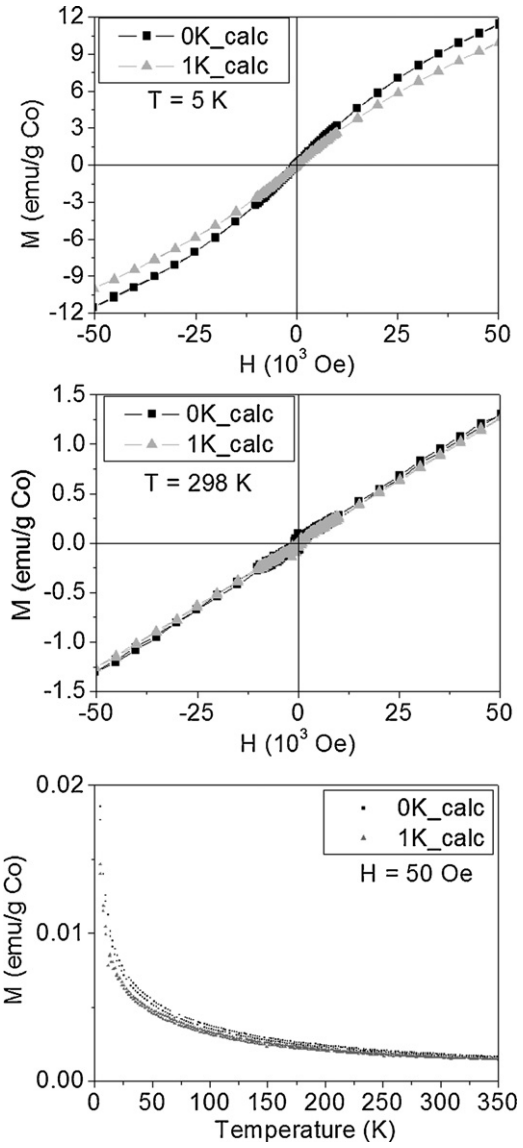

Fig. 6. Magnetization curves vs. applied magnetic field (left and centre) and vs. temperature (right; $H = 50$ Oe) of samples 0K_calc and 1K_calc.

superparamagnetic, matching their high magnetic susceptibility at this temperature, as illustrated in the ZFC–FC curves by the high slope at low temperature. We had previously observed in a set of samples with different Co/Mg/Al molar ratio that the magnetization per gram of cobalt decreased as the amount of cobalt in the hydrotalcite increased, confirming the antiferromagnetic character of the calcined Co/Mg/Al hydrotalcites [10]. ZFC–FC curves appear as superimposed in each sample. The absence of hysteresis excludes the existence of a ferromagnetic phase. Moreover, the absence of inflection points indicates that there is only one magnetic phase, which is assigned to cobalt spinel. Then, and as expected, potassium addition to the hydrotalcites does not alter the magnetic properties of the calcined samples.

3.2. Ethanol steam reforming

Calcined cobalt hydrotalcites, doped with potassium, appear to be active catalysts for the ESR reaction. Monoliths loaded with the same amount of catalyst (150 mg) were tested between 623 K and 823 K with a gaseous H_2O:EtOH molar mixture of 4:1 (steam to carbon, S/C = 2, 8.0×10^{-5} g_{EtOH} min^{-1}). Each temperature was

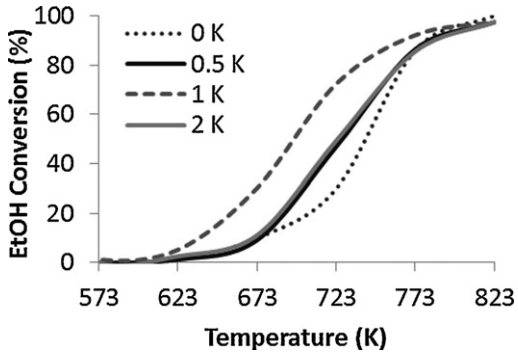

Fig. 7. Ethanol conversion vs. temperature; inlet flow 8.0×10^{-5} g_{EtOH} min^{-1}, S/C = 2.

maintained until the product amount was stabilized after ca. 35 min. Fig. 7 shows the ethanol conversion vs. temperature for the four samples. Ethanol conversion starts to be detectable just above 600 K and reaches total conversion at 823 K. It should be highlighted that as the amount of potassium at the surface increases (determined by XPS), the ethanol conversion is higher at lower temperatures. Therefore, potassium can be regarded as a promoter of the reaction since it enhances the activity of the catalyst.

ESR reaction over cobalt-based catalysts is a complex process that begins with the dehydrogenation of ethanol into acetaldehyde and then follows with the steam reforming of acetaldehyde into hydrogen and a mixture of carbon oxides [7]. The decomposition process of ethanol into methane and carbon monoxide also takes place at high temperature, as well as methanation of carbon oxides. Fig. 8 collects data of product selectivity vs. temperature of the four samples. Below 723 K, the main products are H_2, CH_3CHO, acetone (an undesirable by-product formed at the expenses of acetaldehyde) and CO_2. Above 723 K, the H_2 and CO_2 selectivity increases at the expense of acetaldehyde and acetone. Finally, at 773–825 K oxygenates are consumed and the reverse WGS reaction takes place, with a concomitant increase of CO. Methane and ethylene contents are kept low under the temperature range tested.

As the ethanol conversion vs. temperature is dependent on the amount of potassium, selectivity data at 50% and 100% ethanol conversion have been collected in Fig. 9, in order to study the influence of potassium on the product selectivity (the reaction temperature at 50% EtOH conversion, as depicted from Fig. 7 is 740 K, 725 K, 695 K and 722 K for samples 0 K to 2 K, respectively; the reaction temperature at 100% EtOH conversion is 823 K for the four samples). Hydrogen selectivity increases with potassium addition at 50% EtOH conversion, but it is nearly independent at 100% EtOH conversion. At 50% EtOH conversion, acetaldehyde increases with potassium at the surface (identified by XPS), suggesting that the addition of potassium favours the dehydrogenation of ethanol. At 100% EtOH conversion there is no CH_3CHO, and acetone also diminishes with higher potassium doping. Ethylene selectivity is independent of potassium content, being lower at higher ethanol conversions. Methane and carbon monoxide selectivity are below 2.5% at 50% EtOH conversion, i.e., potassium does not favour the decomposition of ethanol into CH_4 and CO at this temperature. At 100% EtOH conversion, CH_4 selectivity increases slightly due to the higher reaction temperature (823 K).

Stability tests were performed at 823 K during 7 h, with high load of reactants, 0.018 g_{EtOH} min^{-1}, vaporized before entering the reactor (S/C = 2). The four samples were fairly stable during this period of time, reaching 60% of hydrogen selectivity and around 15% of CO_2 content on a dry basis. In order to study in depth how the stability was affected by the addition of potassium, samples 0 K and 1 K were submitted to severer conditions: 200 h of

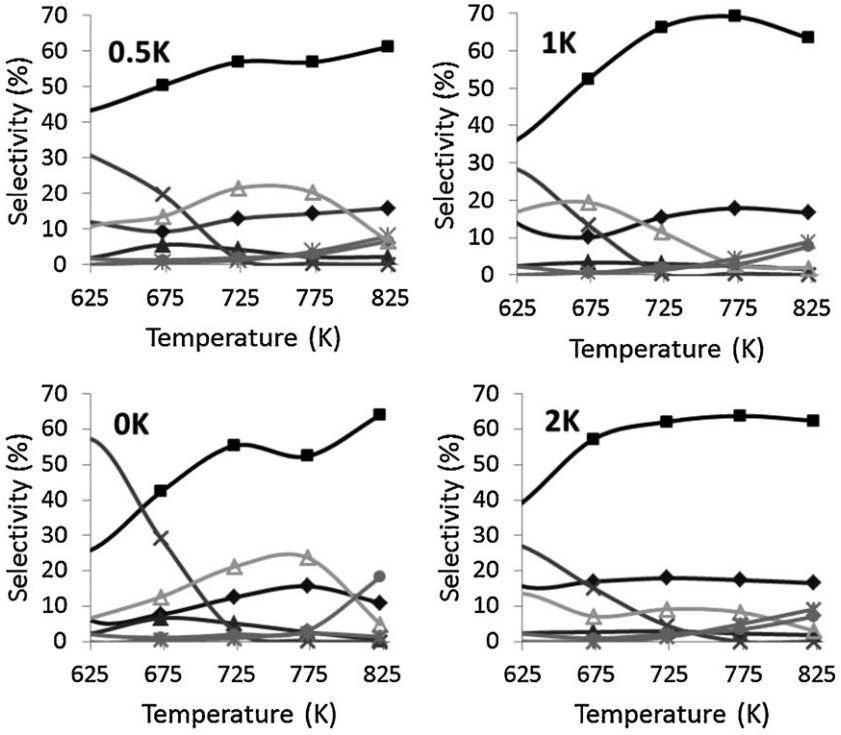

Fig. 8. Product selectivity vs. temperature ((■) H_2, (♦) CO_2, (▲) C_2H_4, (×) CH_3CHO, (△) CH_3COCH_3, (✳) CH_4 and (●) CO); inlet flow 8.0×10^{-5} g_{EtOH} min^{-1}, S/C = 2.

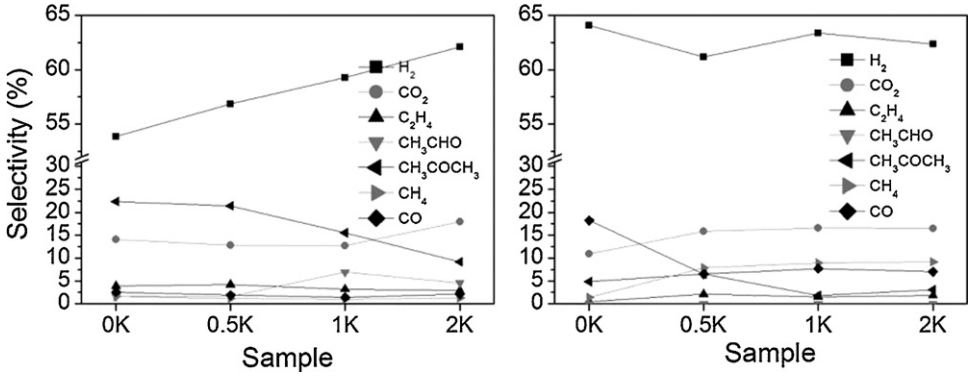

Fig. 9. Product selectivity at 50% EtOH conversion (left: temperature ranges from 695 K to 740 K) and 100% EtOH conversion (right: T = 823 K).

reaction fed with ethanol, followed by 100 h fed with bioethanol (823 K, 0.036 g_{EtOH} min^{-1}; see Fig. 10). Bioethanol contains impurities derived from the fermentation process, which are more difficult to reform than ethanol. Therefore, deactivation of catalysts is faster when fed with bioethanol [22]. Samples 0 K and 1 K were stable during the experiment and showed no significant changes of selectivity when fed either with ethanol or bioethanol (Fig. 10). H_2 selectivity stabilized around 62%, CO_2 around 21%, CO and CH_4 around 5–8%. These values are significantly different from those corresponding to equilibrium (58% H_2, 20.3% CO_2, 18.8% CH_4 and 2.9% CO). In addition, acetaldehyde, which is an intermediate of the ESR process, remained constant in traces along the experiment, indicating that

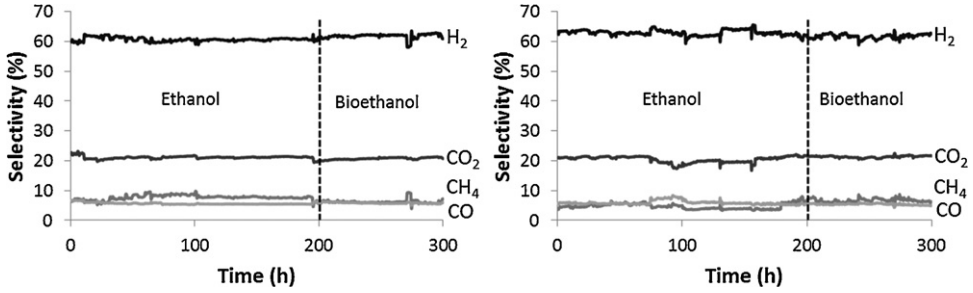

Fig. 10. Stability test: product selectivity vs. time at 823 K with 100% EtOH conversion (left: sample 0 K; right: sample 1 K). Inlet flow 0.036 g_{EtOH} min^{-1}, S/C = 2.

even if ethanol conversion was complete, no deactivation occurred. No acetone, neither ethylene, were produced. It is important to add that the catalytic honeycombs were stable after reaction; the weight loss after exposure to ultrasounds for 30 min was negligible.

The usual lack of stability of cobalt-based catalysts is one of the drawbacks of these materials. Our results are outstanding since our catalysts are stable for at least 200 h under high load of ethanol and a further 100 h under high load of bioethanol, with no signs of deactivation. The disposition of the cobalt atoms within the crystalline structure of the spinel might be determinant for their long-term stability. On the other hand, potassium does not have a significant role in the stability of the catalysts in the time interval studied. The monoliths were weighed before and after the stability tests to monitor the amount of carbon deposited onto the catalysts. Interestingly, no increase of mass was detected in the short-time tests (7 h) in any of the four samples. TPR coupled to mass spectrometry is also a useful tool for identifying carbon formation. Hydrogen reduces coke to methane between 673 K and 1073 K, which can be quantified by a signal at $M = 15^+$ in the mass spectra (the signal $M = 15^+$ corresponds to the radical CH_3^+, the most intense when sampling methane). No peak of mass 15^+ was detected in samples 0K_reac and 1K_reac after stability tests (7 h long), thus again indicating that coke formation was negligible. In the long-time tests (300 h), sample 0 K generated $13.5 \times 10^{-3}\ g_C\ g_{catalyst}^{-1}\ h^{-1}$ and sample 1 K $6.7 \times 10^{-3}\ g_C\ g_{catalyst}^{-1}\ h^{-1}$. These data confirm our initial hypothesis that the addition of potassium to cobalt hydrotalcite-derived catalysts might neutralize the acid sites and, in turn, decrease the coke formation. This fact might favour a better stability in a longer time interval than 300 h, compared to the sample without K.

3.3. Samples after ESR

As we observed in our previous work [10], oxidized cobalt species are active for ethanol steam reforming and, in contrast to metallic cobalt, they are less active but do form a low amount coke during reaction. This constitutes a big advantage on cobalt-based systems for ESR, since these catalysts deactivate easily due to coke formation, although they work at lower temperatures than other metal-based catalysts and they are remarkably cheaper. Here, we have made an effort on the determination of the oxidation state of cobalt after the reaction.

The reacted samples showed simple XRD profiles, with only two peaks (see Fig. 11), corresponding to the rock salt type phase, common to MgO and CoO [15,16] (XRD patterns JCPDS 01-07-1525 and JCPDS 01-075-0533). Any peaks at 47°, 51° neither 53° of 2θ were detected, that would indicate the presence of metallic cobalt. Therefore, the main crystalline phase present in the sample is (Co,Mg)O. Aluminium cations may be highly dispersed in the structure of (Co,Mg)O without the formation of spinel species or, alternatively, be present in an amorphous phase.

XPS analysis shed light on the oxidation state of cobalt atoms at the surface. The spectra of the four samples share the shape and the energy range: there are two main peaks around 781.3 eV and 797.2 eV, which correspond to the Co $2p_{3/2}$/Co $2p_{1/2}$ spin orbital splitting, and two strong satellites (see spectrum of sample 1K_reac in Fig. 12, representative of the four samples). The main peaks, as well as the satellites, could be fitted to only one component. The spin orbital splitting is 15.9 eV and the separation between the satellite lines and the photo lines is close to 5 eV, indicating that the present cobalt species is a high spin Co^{2+}, and practically excluding the existence of Co^{3+} ions. We assign these bands to cobalt oxide (Co,Mg)O. Significantly, there are no peaks at 777–778 eV, indicating again the absence of metallic cobalt at the surface of the catalyst. We had already observed the absence of metallic cobalt under ESR reaction conditions with a Co/Mg/Al calcined hydrotalcite in an in situ XPS experiment [10].

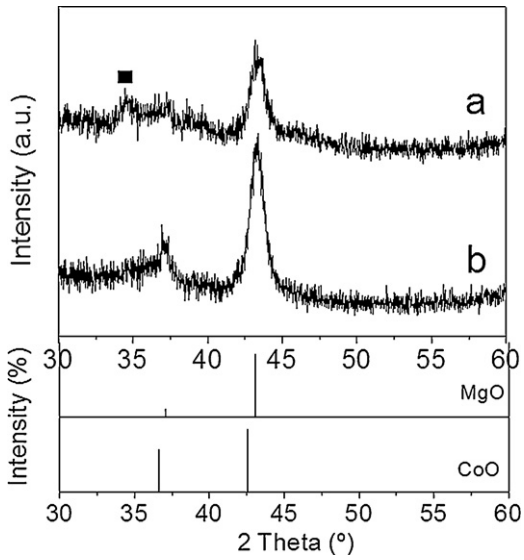

Fig. 11. X-ray diffractograms of reacted samples 0K_reac (a) and 1K_reac (b). (■) Silicon signal from the holder. XRD patterns of several oxide phases are included for comparison.

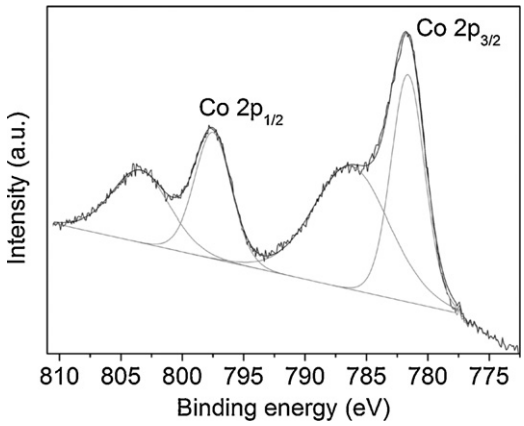

Fig. 12. XP spectrum of sample 1K_reac, representative of the four reacted samples.

The atomic ratio between carbon and cobalt was compared to the amount of potassium in the sample, before and after reaction. The carbon peak has two components. One is assigned to the presence of carbonate species (around 289 eV) and it is not considered for the current calculation. Only the component around 284 eV, assigned to carbon residues, is considered. The values of the C/Co atomic ratios are listed in Table 2. Calcined samples show small C/Co atomic ratio with an average value of 1.4. After reaction, the C/Co atomic ratio increased significantly (one order of magnitude, from 1.1 to 10.8) in sample 0K_reac. On the other hand, the samples doped with potassium do not show such a high C/Co atomic ratio

Table 2
Co and C atomic composition at the surface of calcined and reacted samples calculated by XPS.

Calcined samples	C/Co (atomic ratio)	Reacted samples	C/Co (atomic ratio)
0K_calc	1.1	0K_reac	10.8
0.5K_calc	1.2	0.5K_reac	5.2
1K_calc	0.2	1K_reac	5.1
2K_calc	3.3	2K_reac	4.0

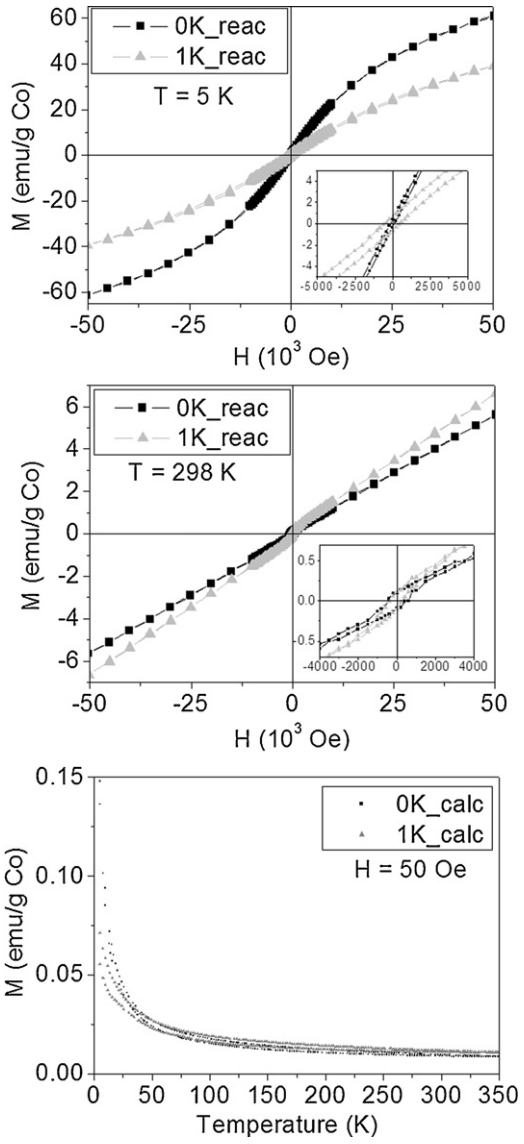

Fig. 13. Magnetization curves vs. applied magnetic field (left and centre) and vs. temperature (right, $H = 50$ Oe) of samples 0K_reac and 1K_reac.

after reaction, reaching values only 4.0–5.2. These results indicate, once more, that the presence of potassium in the sample hinders the formation of coke during ethanol steam reforming.

The magnetic measurements point towards the existence of two magnetic phases after reaction. The main one has a paramagnetic profile, indicated by the linear increase of magnetization at room temperature as the applied magnetic field is intensified. The minor one is related with a slight superparamagnetic shape at 5 K, and also by the decrease in magnetization as the temperature increases in the zero field cooled–field cooled experiments (see Fig. 13). That profile matches with an antiferromagnetic behaviour, for what we assign it to the cobalt oxide phase. The second phase is ferromagnetic, as evidenced by the small hysteresis at low applied magnetic field, both at 5 K and at RT. We have assigned this phase to metallic cobalt. Its amount, calculated as the percentage ratio between the experimental saturation magnetization (5.6 and 6.6 emu/g) and the bulk saturation magnetization (163 emu/g) at room temperature, is only 0.09 wt.% and 0.18 wt.%, for samples 1K_reac and 0K_reac, respectively. It can be argued that the lack of metallic cobalt could be attributed to a reoxidation of the metallic cobalt entities potentially formed during the ESR. However, we had observed in a previous work on cobalt talc nanolayers, that the catalyst after

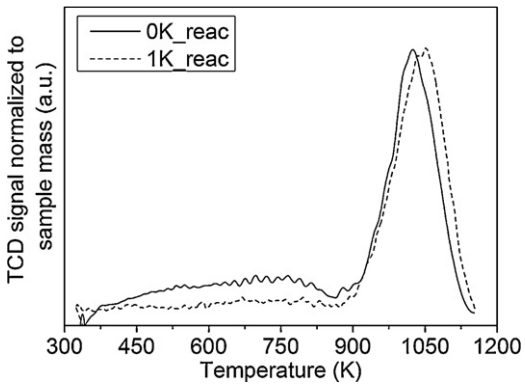

Fig. 14. TPR profiles of samples 0K_reac and 1K_reac.

reaction showed clearly ferromagnetic behaviour in the magnetization curves vs. field and vs. temperature. In that case, the sample was kept at normal conditions, indicating that Co^0 entities were stable under these conditions and they were not reoxidized [23].

TPR profiles recorded after ESR reaction show only one peak, centred at 1013 K and 1043 K, for samples 0K_reac and 1K_reac, respectively (see Fig. 14). These peaks correspond to the reduction of Co^{2+} to Co^0. There is no peak around 700 K, confirming that Co^{3+} species are not present after the reaction, as observed by XRD, XPS and magnetic measurements. This is due to the reduction of Co^{3+} in cobalt spinel by the hydrogen generated during ESR, which was carried out at 823 K (compare the TPR profiles before and after ESR, Figs. 5 and 14, respectively). Therefore, only Co^{2+} is present in the sample. The peaks are narrow and well defined, pointing to a homogeneous dispersion of the Co^{2+} species in the material.

4. Conclusions

We have synthesized a new family of robust honeycomb catalysts for bioethanol steam reforming based on calcined Co/Mg/Al hydrotalcites doped with potassium. The addition of potassium to the hydrotalcites reduces the number and strength of acid sites. The catalysts are active for the ESR reaction, where potassium acts as a promoter, being very stable for long-term experiments under high loads of both ethanol and bioethanol and generating little carbon (0.0067 $g_C\ g_{catalyst}^{-1}\ h^{-1}$). During reaction, cobalt spinel transformed completely into high spin Co^{2+} in cobalt oxide (or in (Co,Mg)O) and only traces of metallic cobalt were identified by magnetometry, <0.1 wt.% Co^0, indicating that oxidized cobalt is an active species in ESR.

Acknowledgements

This work has been funded by MICINN project CTQ2009-12520. R.E. is grateful to CONACYT México for a PhD grant and E.T. to UPC for a postdoc grant. F.M. and J.L. are grateful to ICREA Academia program.

References

[1] H. Idriss, M. Scott, J. Llorca, S.C. Chan, W. Chiu, P.Y. Sheng, A. Yee, M.A. Blackford, S.J. Pas, A.J. Hill, F.M. Alamgir, R. Rettew, C. Petersburg, S.D. Senanayake, M.A. Barteau, ChemSusChem 1 (2008) 905–910.
[2] P. Bichon, G. Haugom, H.J. Venvik, A. Holmen, E.A. Blekkan, Topics in Catalysis 49 (2008) 38–45.
[3] J. Llorca, P.R. de la Piscina, J.A. Dalmon, J. Sales, N. Homs, Applied Catalysis B: Environmental 43 (2003) 355–369.
[4] J. Llorca, J.A. Dalmon, P.R. de la Piscina, N. Homs, Applied Catalysis A: General 243 (2003) 261–269.
[5] J. Llorca, N. Homs, P.R. de la Piscina, Journal of Catalysis 227 (2004) 556–560.
[6] A.M. Karim, Y. Su, M.H. Engelhard, D.L. King, Y. Wang, ACS Catalysis 1 (2011) 279–286.

[7] A. Casanovas, C. de Leitenburg, A. Trovarelli, J. Llorca, Chemical Engineering Journal 154 (2009) 267–273.
[8] G. Busca, U. Costantino, T. Montanari, G. Ramis, C. Resini, M. Sisani, International Journal of Hydrogen Energy 35 (2010) 5356–5366.
[9] A.M. Karim, Y. Su, J. Sun, C. Yang, J.J. Strohm, D.L. King, Y. Wang, Applied Catalysis B: Environmental 96 (2010) 441–448.
[10] R. Espinal, E. Taboada, E. Molins, R.J. Chimentao, F. Medina, J. Llorca, RSC Advances 2 (2012) 2946–2956.
[11] J.F. da Costa-Serra, A. Chica, International Journal of Hydrogen Energy 36 (2011) 3862–3869.
[12] F. Cavani, F. Trifiro, A. Vaccari, Catalysis Today 11 (1991) 173–301.
[13] T. Yamanaka, Y. Takeuchi, Zeitschrift Fur Kristallographie 165 (1983) 65–78.
[14] P.G. Casado, I. Rasines, Journal of Solid State Chemistry 52 (1984) 187–193.
[15] E. Schiebold, Z. Kristallographie, Kristallgeometrie, Kristallphysik, Kristallchemie 56 (1921) 430.
[16] W.D. Johnston, R.R. Heikes, D. Sestrich, Journal of Physics and Chemistry of Solids 7 (1958) 1–13.
[17] I. Boz, Catalysis Letters 87 (2003) 187–194.
[18] M. Nagai, K. Koizumi, S. Omi, Catalysis Today 35 (1997) 393–405.
[19] J.Y. Shen, M. Tu, C. Hu, Journal of Solid State Chemistry 137 (1998) 295–301.
[20] P. Kustrowski, L. Chmielarz, E. Bozek, M. Sawalha, F. Roessner, Materials Research Bulletin 39 (2004) 263–281.
[21] J. Rass-Hansen, R. Johansson, M. Moller, C.H. Christensen, International Journal of Hydrogen Energy 33 (2008) 4547–4554.
[22] A.A. Khassin, T.M. Yurieva, V.V. Kaichev, V.I. Bukhtiyarov, A.A. Budneva, E.A. Paukshtis, V.N. Parmon, Journal of Molecular Catalysis A: Chemical 175 (2001) 189–204.
[23] M. Dominguez, E. Taboada, H. Idriss, E. Molins, J. Llorca, Journal of Materials Chemistry 20 (2010) 4875–4883.